Integrative and Comparative Biology

Integrative and Comparative Biology, volume 53, number 2, pp. 269–282
doi:10.1093/icb/ict067

Society for Integrative and Comparative Biology

SYMPOSIUM

A Salamander's Flexible Spinal Network for Locomotion, Modeled at Two Levels of Abstraction

Jeremie Knüsel,[1,*] Andrej Bicanski,[*] Dimitri Ryczko,[†] Jean-Marie Cabelguen[‡] and Auke Jan Ijspeert[*]

[*]Biorobotics Laboratory, School of Engineering, École Polytechnique Fédérale de Lausanne, Station 14, CH 1015 Lausanne, Switzerland, [†]Groupe de Recherche sur le Système Nerveux Central, Département de physiologie, Université de Montréal, C.P. 6128, succursale centre-ville, Montréal, Québec, Canada H3C 3J7 and [‡]INSERM U862, Neurocentre Magendie, Motor System Diseases Group, Université de Bordeaux, 146 rue Léo Saignat, 33077 Bordeaux Cedex, France

From the symposium "Vertebrate Land Invasions – Past, Present, and Future" presented at the annual meeting of the Society for Integrative and Comparative Biology, January 3–7, 2013 at San Francisco, California.

[1]Email: jeremie.knuesel@epfl.ch

Synopsis Animals have to coordinate a large number of muscles in different ways to efficiently move at various speeds and in different and complex environments. This coordination is in large part based on central pattern generators (CPGs). These neural networks are capable of producing complex rhythmic patterns when activated and modulated by relatively simple control signals. Although the generation of particular gaits by CPGs has been successfully modeled at many levels of abstraction, the principles underlying the generation and selection of a diversity of patterns of coordination in a single neural network are still not well understood. The present work specifically addresses the flexibility of the spinal locomotor networks in salamanders. We compare an abstract oscillator model and a CPG network composed of integrate-and-fire neurons, according to their ability to account for different axial patterns of coordination, and in particular the transition in gait between swimming and stepping modes. The topology of the network is inspired by models of the lamprey CPG, complemented by additions based on experimental data from isolated spinal cords of salamanders. Oscillatory centers of the limbs are included in a way that preserves the flexibility of the axial network. Similarly to the selection of forward and backward swimming in lamprey models via different excitation to the first axial segment, we can account for the modification of the axial coordination pattern between swimming and forward stepping on land in the salamander model, via different uncoupled frequencies in limb versus axial oscillators (for the same level of excitation). These results transfer partially to a more realistic model based on formal spiking neurons, and we discuss the difference between the abstract oscillator model and the model built with formal spiking neurons.

Introduction

Animals change gait to locomote at different speeds or in different environments or to reach specific goals, each gait being characterized by a specific pattern of activation of the muscles. In both invertebrates and vertebrates, the proper coordination of muscles for locomotion relies to a large extent on neural networks called central pattern generators (henceforth CPGs), which are capable of generating coordinated rhythmic outputs from simple input signals such as tonic excitation (Grillner 2006). The CPG networks for locomotion in vertebrates are located in the spinal cord and are modulated by descending commands from the brain stem and by sensory feedback (Rossignol et al. 2006; Ryczko and Dubuc 2013).

Here, we consider possible designs for a flexible salamander's CPG capable of generating a wide range of intersegmental coordination patterns. As one of the living animals closest to early tetrapods—its morphology has been relatively stable for the past 150 million years (Gao and Shubin 2001)—and as an amphibian, the salamander is a good candidate for investigating the neural and morphological changes that accompanied the transition of vertebrates from aquatic habitats to land. Its nervous

Advanced Access publication June 18, 2013

system is relatively simple for a tetrapod (Nieuwenhuys et al. 1998), showing remarkable similarities to that of the lamprey (Ryczko et al. 2010b), a primitive jawless fish that uses an anguilliform swimming gait close to that of the salamander. These similarities allow us to build on the vast literature on lampreys. The lamprey has one of the best-documented and most extensively modeled central nervous systems among vertebrates. The relative simplicity of its nervous system makes modeling studies more tractable, and yet much of the knowledge gained can be used as a guide to understand the locomotor network of other vertebrates (Grillner 2003).

Modeling work on salamander locomotion has concentrated on swimming and forward stepping on land. During swimming, electromyographic recordings of epaxial muscles show waves of muscle activation traveling from the head to the tail and alternating between the left and right sides of the body, while during forward stepping on land, a synchronous activation of ipsilateral muscles (i.e., a standing wave) is typically observed in the trunk (Frolich and Biewener 1992; Delvolvé et al. 1997). However, experimental data indicate that the salamander's spinal networks are capable of a large diversity of intersegmental coordination patterns in the isolated spinal cord (Ryczko et al. 2009) and in the intact animal (Cabelguen et al. 2010). For example, rostrocaudal traveling waves are sometimes observed in the trunk during forward stepping.

The similarities between lampreys and salamanders have led to the notion that the organization of the lamprey's nervous system can serve as a blueprint for the axial networks of the salamander. This has been exploited in various modeling studies, which posit that a lamprey-like swimming circuit is augmented with neural networks that govern limb movements (Bem et al. 2003; Ijspeert et al. 2005; Ijspeert et al. 2007; Harischandra et al. 2011; for a review, see Bicanski et al. 2013a).

Harischandra et al. (2011) have studied the transitions between two stepping gaits: a walking gait with traveling waves of muscle activation in the trunk (similar to the swimming pattern) and the usual walking trot, with standing waves in the trunk. In their model, the transitions between the traveling wave and standing wave patterns in the trunk were governed by the connections from limb to axial oscillators. These connections were global, that is, targeting all axial oscillators, and imposed a standing wave in the trunk during trotting. The connections were weakened during the walking gait to allow the formation of a traveling wave of activity in the trunk. This mechanism for the selection of a traveling or standing wave is similar to that used in the work of Ijspeert et al. (2007), in which connections from limb to axial oscillators are silent during swimming as the limb oscillators are saturated, but active during forward stepping. In both studies, the extensive couplings from limb to axial oscillators (Fig. 1A) lead to a poor flexibility of the trunk and tail activity patterns when the limb oscillators are active, as each limb oscillator forces synchronous oscillations in all of the oscillators to which it projects.

In the model of Ijspeert et al. (2007), the axial network is also rigid by itself. This is in contrast to recent lamprey models, in which an adjustment of the excitation at one end of the cord can be used to increase or decrease the intersegmental phase-lag while keeping it uniform along the body (Kozlov et al. 2009). The axial network in Fig. 1A would require adjusting the uncoupled frequency at both ends of the chain in opposite amounts. An adjustment at only one end would give a gradient of phase-lags along the cord (Cohen et al. 1982).

We investigated two solutions that may rectify the above shortcomings of earlier models. One is a network in which the couplings do not constrain the value of the intersegmental phase-lag but simply ensure that it is uniform along the cord. The second is inspired by recent models of the lamprey CPG, which include an asymmetry between rostrocaudal and caudorostral intersegmental couplings. In this approach, we show how the introduction of asymmetric intersegmental couplings in combination with local couplings between limb and axial oscillators (Fig. 1D) yields a flexible CPG network, in which the uncoupled frequency of the limb oscillators affects the intersegmental phase-lags along the cord. This holds true at two levels of abstraction, in an oscillator network and in a network composed of formal spiking neurons, which operates on principles inspired by biologically detailed models (Bicanski et al. 2013b). The uniformity of intersegmental phase-lags in the networks of the mid-trunk and tail is preserved. Finally, we show that this mechanism can account for the transition of gait between swimming and stepping at both levels of abstraction.

Methods

The oscillator model

The oscillator model is built on abstract phase oscillators with controlled amplitude. The dynamics of

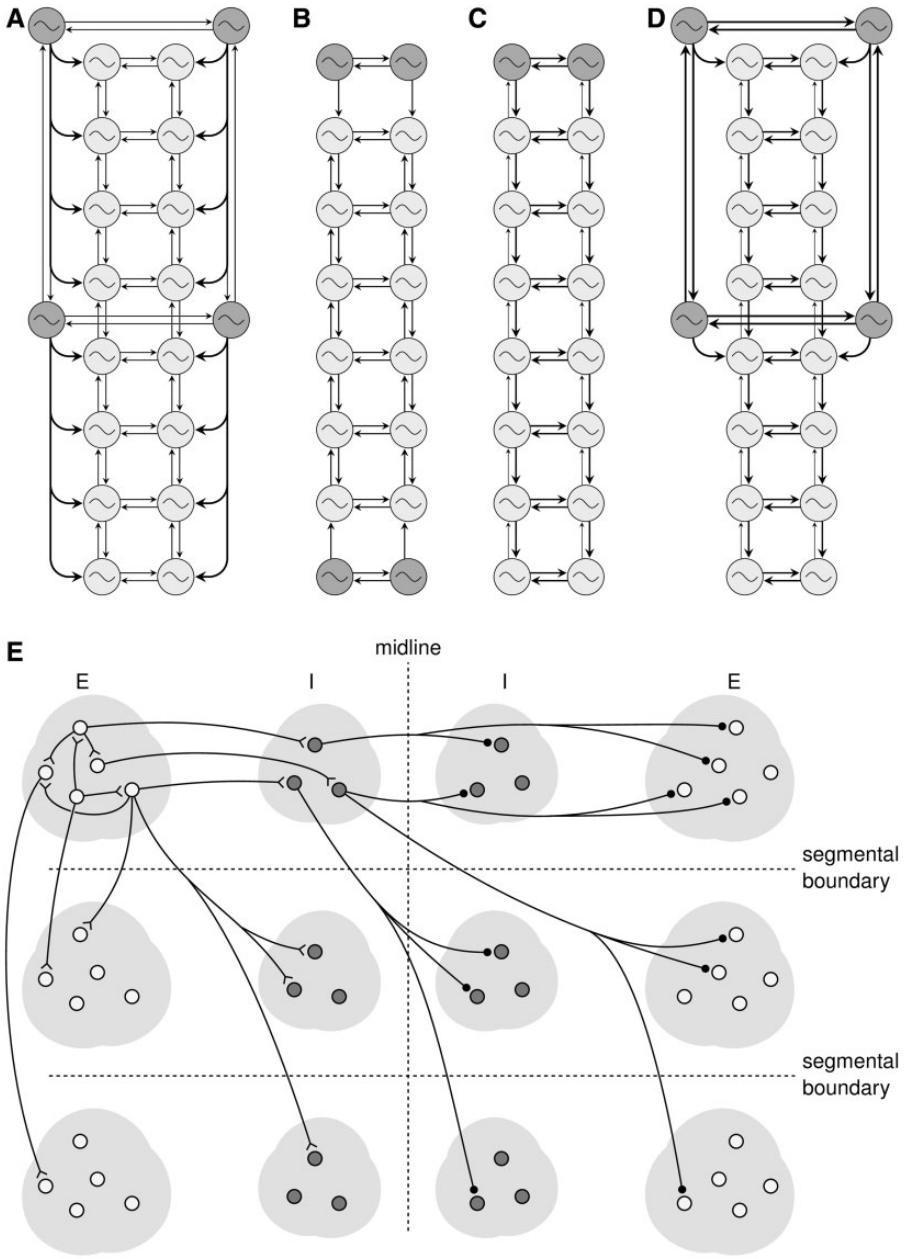

Fig. 1 Network topologies. Thicker arrows in (**A–D**) indicate stronger couplings. (A) Full salamander network configuration in the abstract oscillator model of Ijspeert et al. (2007), with global couplings from limb (dark gray) to axial (light gray) oscillators. (B) An example connectivity for an axial CPG that allows for arbitrary intersegmental phase-lags as part of the network state. The phase-lag can be controlled through transient perturbations applied to one of the boundary segments (dark gray oscillators). (C) Axial network with dominantly descending intersegmental couplings. The intersegmental phase-lag can be adjusted by varying the uncoupled frequency of the first segment (dark gray) relative to other oscillators, as in lamprey models (Kozlov et al. 2009). (D) Full salamander network using local projections from limb (dark gray) to axial (light gray) oscillators and dominantly descending intersegmental couplings. (**E**) Schematic representation of the default connectivity (descending intersegmental couplings only) within and among segments in the integrate-and-fire model. Note that the full model consists of 16 axial segments and 2 limb segments (one half-center per limb). Limb segments do not receive connections from the axis. Diagonally opposed half-centers are coupled with inhibitory connections. Excitatory neurons (E) and inhibitory neurons (I) are represented in light and dark gray, respectively. Only connections originating from the upper-left quadrant (i.e., originating from one hemisegment) are shown. See Table 3 for densities of all connections.

each oscillator is described by the following equations:

$$\dot{\theta}_i = 2\pi\nu_i + \sum_j w_{ij} r_j \sin(\theta_j - \theta_i - \varphi_{ij}) \quad (1)$$

$$\dot{r}_i = a(R_i - r_i) \quad (2)$$

$$x_i = r_i(1 + \cos\theta_i) \quad (3)$$

Here, θ_i is the phase of oscillator i (the phase of an uncoupled oscillator increases linearly). The oscillatory output x_i is calculated from the cosine of the phase and is maximal when the phase is a multiple of 2π. r_i is the amplitude, ν_i the uncoupled frequency, R_i the target amplitude, and a is a constant. The coupling from oscillator j to oscillator i is characterized by a weight w_{ij} and phase bias φ_{ij}. Different connectivities were considered as described in the 'Results' section and illustrated in Fig. 1A–D; arrows in the figure correspond to nonzero weights w_{ij} in the corresponding coupling term of Equation (1). The phase bias φ_{ij} for intersegmental couplings depends on the model, but for couplings between two axial oscillators in the same segment or between two limb oscillators, it is always π (i.e., 50% of a cycle) in order to maintain an antiphase relationship.

The neuron model

The formal spiking neuron model is a standard integrate-and-fire (henceforth IF) neuron, extended by adaptation variables [see Equation (4)], where u denotes the membrane potential, g the leak conductance, and E_{rest} the resting potential. The two adaptation variables (ω_i) act on different time scales (in the order of 100 ms versus 1000 ms) and are scaled by constants α_i. I and R are the input current and the input resistance. The sum indicates the summation of all synaptic currents (*syn* stands for NMDA, AMPA or GLYC), with g_{syn} the synaptic conductance and w_{syn} the synaptic weight.

$$\begin{aligned}\tau\dot{u} = &-g(u - E_{rest}) - \alpha_1\omega_1 - \alpha_2\omega_2 + RI \\ &+ \sum w_{syn} g_{syn}(u - E_{revsyn})\end{aligned} \quad (4)$$

$$\tau_{w_i}\dot{\omega}_i = -\omega_i \quad (5)$$

$$\tau_{syn}\dot{g}_{syn} = -g_{syn} \quad (6)$$

When the neuron reaches the firing threshold, the spike time is recorded, the membrane potential is reset, and the adaptation variables are incremented by $\Delta\omega_i$ with each spike and then decay exponentially [see Equation (5)]. After a spike, the neuron is clamped to the resting membrane potential value for a refractory period of 5 ms. Inhibitory and excitatory synaptic conductances are incremented by Δg_{syn} after each received spike and are also subject to exponential decay, as per Equation (6) (Vogels and Abbott 2009). Inspired by the modeling studies on the lamprey (Tråvén et al. 1993), and recently the salamander (Bicanski et al. 2013b), excitatory postsynaptic potentials have a slowly decaying N-methyl-D-aspartic acid (NMDA)-like component and a fast (±)-α-amino-3-hydroxy-5-methylisoxazole-4-propionic acid (AMPA)-like component. All neuron parameters are summarized in Table 2. Synaptic weights are given in Table 3.

The IF network

Figure 1E depicts the segmental and intersegmental organization of the basic IF network model for the salamander's spinal CPG used in this study. Each side of the symmetric segmental network consists of 25 sparsely interconnected excitatory neurons, which drive a population of 20 inhibitory neurons, which in turn project to the contralateral side of the segment. The connection densities within the salamander's spinal networks are unknown and have been treated as open parameters. The ratio between the number of excitatory and inhibitory neurons was inspired by the work of Cheng et al. (2002). Recent experimental data suggest that excitatory cross-connections exist between half-centers (Ryczko et al. 2010a). It is unknown whether these target contralateral excitatory interneurons or contralateral motoneurons in the salamander (for the lamprey, see Buchanan 1982; Buchanan and McPherson 1995; for review, see Ryczko et al. 2010b).

In the present study, we omit motoneurons and the commissural excitatory connections. The axial network consists of 16 identical segments. Intersegmental connections from ipsilateral excitatory neurons and contralateral inhibitory neurons extend only caudally in the default network (network 1, see Table 3). The limb oscillators are implemented as two separate segmental networks (Note that these simplified limb oscillators only generate the rhythm of the limb networks. Actual limb centers that control multi-joint limbs require more complex networks). Half-centers of the limbs project only to the nearest two axial segments, with decreasing connection probability. Limb-to-axis connections are inhibitory toward the contralateral side and excitatory toward the ipsilateral side. Variants of the default network include ascending intersegmental connections in the axis (network 2, see Table 3) and two variants of network 2 with slight modifications of the connectivity (networks 3 and 4, see Table 3) that help recover the performance of the

default network. All parameters are summarized in Table 3.

Quantification of gait parameters

The patterns of activity of the various networks are characterized by measuring two quantities: the oscillation or bursting frequency and the phase-lag between the oscillations or bursts in consecutive segments. In the IF model, spikes are counted at each time-step and for each hemisegment. A cubic spline fit from the Mathworks Matlab spline toolbox (function csaps) is applied to obtain a smooth signal. A heuristic algorithm is used to determine the onset and offset of each burst, as described in Fig. 2. The timing of the burst is calculated from the centroid of the surface enclosed by the onset, the offset, and the spline curve. The same method is applied to the output signal of the oscillators, without the spline filtering, since no spikes are present in this case. The zero-crossings of the oscillations are used as onsets and offsets.

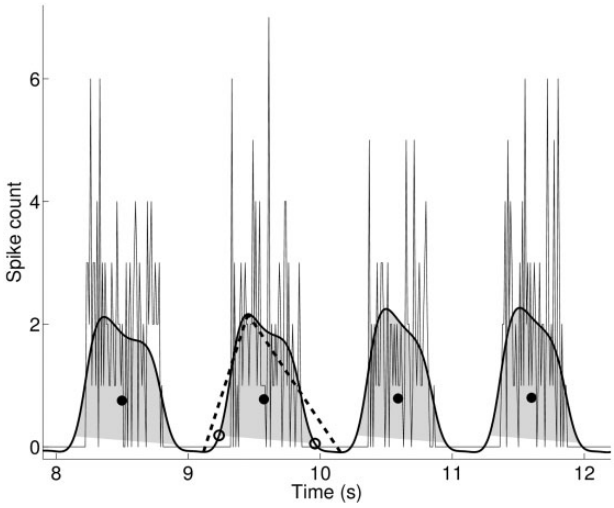

Fig. 2 Automated processing of spike data generated by the IF model. The number of spikes in a hemisegment is counted at each time-step of 1 ms (thin black line, only one tenth of data points shown for clarity) and filtered with a cubic spline fit (thick black line). The onset and offset of each burst are estimated by tracing a line from the local maximum to the local minimum on each side (dashed lines) and finding the points on the spline curve that are furthest away from these lines (open markers). The burst time is calculated as the centroid (filled marker) of the surface delimited by the spline curve and the two open markers.

Results and discussion

In the following, we present our iterative approach to modeling a flexible salamander's CPG, starting with the more abstract models.

The coordination pattern as a network state

CPGs are traditionally conceived as producing a specific pattern of activity for given inputs from the brain and sensory feedback. In the case of multistable networks, the same parameters can support a few different patterns of activity and a transient perturbation of the network state suffices to switch from one pattern to another (Briggman and Kristan 2008).

Here, we extend this notion of multistability and consider the speculative hypothesis that the CPG network might support a continuum of coordination patterns. In the case of the salamander's axial CPG, the role of the intersegmental couplings would then not be to establish a particular phase-lag, but to ensure the uniformity of the phase-lag—any phase-lag—in a part of the spinal cord (e.g., the mid-trunk or the tail). Such a network would store the intersegmental phase-lag as part of its state. The phase-lag could be altered at any time by perturbing a part of the network, causing a modification of the local phase-lag that the couplings would then replicate in the rest of the network.

In the abstract oscillator framework, we can explicitly design a network with this property. Restricting the analysis to the axial CPG, we can use, for example, the axial network of Fig. 1B, with identical coupling weights w_{ij} and phase biases $\varphi_{ij} = 0$ for all intersegmental couplings (i.e., symmetrical ascending and descending couplings). Note that compared with the axial network of Fig. 1A, we have removed couplings from the second segment to the first segment, and from the second-to-last segment to the last segment. As a result, every oscillator receives either no intersegmental coupling (first and last segment, dark gray oscillators) or couplings both from their rostral and caudal neighbor. Both couplings have the effect of "pulling" the receiver to oscillate in phase with the sender. The effect is strongest for the coupling from the oscillator that has the largest phase difference to the receiver. The receiver will thus be attracted toward this oscillator until the attraction from the caudal and rostral neighbors is balanced, that is, until the phase-lag from the rostral neighbor to the receiver equals the phase-lag from the receiver to the caudal neighbor. The couplings thus have the desired effect of establishing a uniform intersegmental phase-lag along the cord, without constraining the actual value of the phase-lag. Instead, the phase-lag is determined by the phase of the oscillators in the first and last segments, which receive no coupling from other segments: the sum of the intersegmental phase-lags established by the network will be equal to the

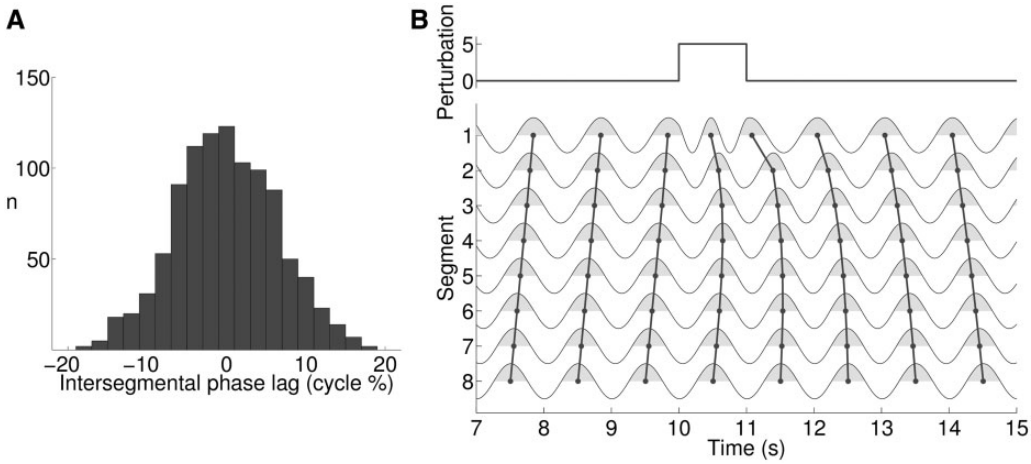

Fig. 3 (**A**) Distribution of phase-lags obtained with 1000 simulations of the network of Fig. 1B and random initial conditions, with $\nu_i = 1$ and $R_i = 1$ for all oscillators, $w_{ij} = 5$ and $\varphi_{ij} = 0$ for all couplings, and $a = 1$. For each simulation, the mean and standard deviation across positions along the cord and across all oscillations were calculated. (**B**) The bottom part of the figure shows the output of the left oscillator in each segment (thin black lines) and the area used to calculate the timing of the oscillation (light gray). The lag between consecutive segments is illustrated with thick black lines. A transient perturbation of 1 s applied to the first segment (top part of the figure) makes the network switch from negative to positive phase-lags.

difference in phase between the first and last segment, modulo 2π. The distribution of intersegmental phase-lag produced by the network is shown in Fig. 3A. The phase-lag can be changed by perturbing one of the boundary segments. This provides a simple mechanism for the control of the oscillation pattern. For example, Fig. 3B illustrates how a transient perturbation to the first segment can be used to obtain a different oscillation pattern. Here, the perturbation is added to the derivative of the phase variable in Equation (1). A positive value accelerates the first segment and thus increases the phase-lag to the second oscillator, which will be replicated by the couplings in the rest of the network. A longer perturbation will yield an even higher phase-lag between the first and second oscillators, and eventually a higher intersegmental phase-lag in the whole network.

A lamprey-inspired flexible network

We present here an alternative design for a flexible CPG network. The design is more conventional than that of the previous section, being directly inspired by models of the lamprey CPG. Using a detailed simulation of the lamprey CPG based on the Hodgkin–Huxley formalism, Kozlov et al. (2009) showed that the intersegmental phase-lag could be increased or decreased by adjusting the amount of excitation provided to the first CPG segments, compared with the rest of the spinal cord. However, they mention that an asymmetry in the rostrocaudal versus caudorostral intersegmental couplings (using more extensive projections in the rostrocaudal direction) is important for maintaining a uniform phase-lag along the body. A schematic representation of a lamprey network with asymmetrical couplings is shown in Fig. 1C.

Table 1 Parameter values for the lamprey-inspired oscillator model of Fig. 1D

e_i	1 (axial oscillators) 0.5 (limb oscillators)
d_i^{th}	5 (axial oscillators) 2.5 (limb oscillators)
w_{ij}	5 (lateral and descending couplings) 1 (ascending couplings)
φ_{ij}	11.1% (descending couplings) −11.1% (ascending couplings)
a	5

In the model of Fig. 1B, transient perturbations to the first oscillators were sufficient to change durably the intersegmental phase-lag in the whole network. In the model of Fig. 1C, however, a persistent increase or decrease of the intrinsic frequency of the first oscillators is required to maintain a higher or lower intersegmental phase-lag, respectively. As soon as the adjustment is removed, the phase-lag will revert to the nominal value $\varphi_{ij.}$

We built a model of the salamander CPG based on the second principle (Fig. 1C), by taking the network of Fig. 1A and not only removing most of the couplings from limb to axial oscillators but also introducing an asymmetry in the intersegmental couplings by using five times higher coupling weights in the

rostrocaudal direction (Fig. 1D). The parameter values are given in Table 1. Using different uncoupled frequencies for the limb and axial oscillators in this network results in a continuous range of phase-lags and oscillation frequencies, as shown in Fig. 4.

The mechanism of intersegmental phase-lag modulation can be understood intuitively. With caudorostral couplings being weaker than rostrocaudal couplings, a segment will entrain a slower caudal neighbor to a frequency close to its own. However, the slower segment will only follow the faster one after a delay, increasing the phase-lag between the two segments. This effect propagates along the axis, ensuring a uniform frequency and phase-lag in the whole chain. The effect of a slow segment on a faster caudal neighbor is similar, except in that it is now the rostral segment that will lag on the caudal one, causing a decrease in the phase-lags, which can even become negative.

This mechanism regulates the phase-lag in a similar manner to the trailing oscillator hypothesis proposed for the lamprey CPG (Matsushima and Grillner 1992). However, in this work the authors proposed equivalent couplings in rostrocaudal and caudorostral directions. In the present model, we find that in order to maintain a uniform phase-lag along the chain of oscillators, asymmetric couplings are important. Symmetric intersegmental couplings would lead to an attenuation of the effect of the frequency difference as it propagates down the axis, since a segment would not adapt to the frequency of its rostral neighbor, but rather a value between its intrinsic frequency and that of its neighbor. As a consequence, nonuniform phase-lags develop along the axis. To obtain uniform phase-lags, one has to adjust the uncoupled frequency of the first and last segments in opposite amounts (Cohen et al. 1982).

As mentioned previously, the lamprey model of Kozlov et al. (2009) showed similarly that intersegmental coupling asymmetry was important to generate a uniform phase-lag along the cord. There is ample experimental evidence for such asymmetry in the lamprey, though there is conflicting evidence regarding the direction of the dominant couplings (Hill et al. 2003). In the model of Kozlov et al. (2009), a lasting increase or decrease of the excitation to the first segments is used to select between forward and backward swimming, that is, between positive and negative intersegmental phase-lags (Fig. 1C). In our model, this adjustment of the excitation is replaced by the influence of the limb oscillators on the first axial segment (Fig. 1D). Using different frequencies for the limb and axial oscillators, we can control independently the frequency and intersegmental phase-lag in the network (Fig. 4).

Selection of a model based on experimental data

The network of Fig. 1B is very sensitive to perturbations of the phase or uncoupled frequency of the boundary oscillators. A slight difference in the frequency of a sensitive oscillator would lead to a continuous drift in phase-lags (Fig. 3B). This is in contradiction with the observation in the lamprey that local sensory feedback can entrain the whole network to the frequency of mechanical oscillations applied at one end (McClellan and Sigvardt 1988; Williams et al. 1990). Moreover, recordings from isolated salamander spinal cords

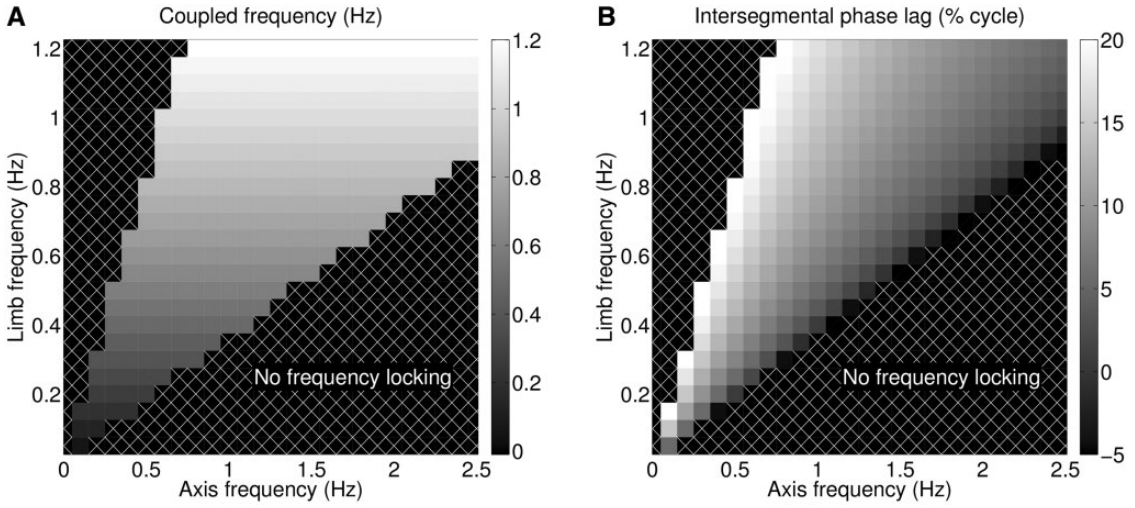

Fig. 4 Frequency and phase-lag in the flexible oscillator model. The network frequency (**A**) and intersegmental phase-lag (**B**) in the network of Figure 1D can be adjusted independently by varying the uncoupled frequency of the axial and limb oscillators (horizontal and vertical axes, respectively). The network frequency is determined by the uncoupled frequency of the limb centers. The phase-lag increases with increasing limb frequencies and decreases with increasing axial frequencies. White crosses on black background indicate parameter values for which the limb and axial oscillators would not reach frequency locking.

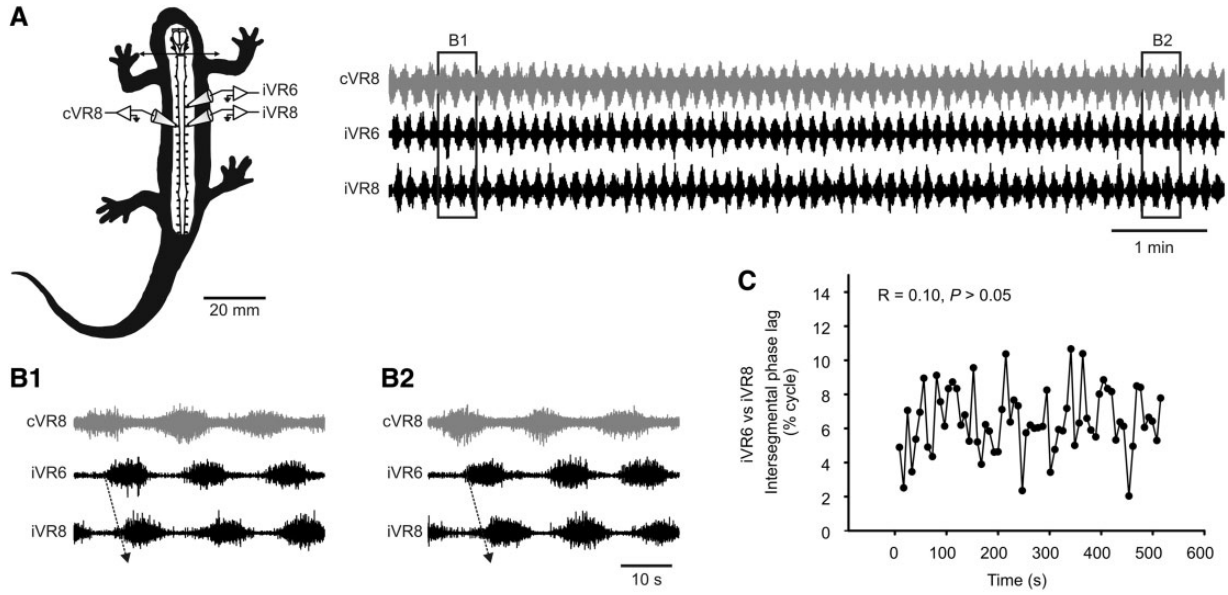

Fig. 5 The salamander spinal cord generates stable phase-lags. (**A)** Typical rostrocaudal waves of axial activity of two ipsilateral (iVR6 and iVR8) and one contralateral (cVR8) ventral roots of the isolated spinal cord of *Pleurodeles waltlii* were recorded when pharmacologically activated by NMDA (20 μM) and D-serine (10 μM) (see Ryczko et al. 2010a for methods). (**B1** and **B2)** Magnification of two parts of the recordings in A. (**C**) Plot of intersegmental phase-lag recorded between VR6 and VR8 versus time revealed no significant correlation, indicating a stable phase-lag.

show cycle-to-cycle variabilities in phase-lags but no systematic drift (Fig. 5, see also Ryczko et al. 2010a). Such stable phase-lags would be unlikely if the slightest difference in uncoupled frequencies between the boundary and middle segments of the preparation were to cause a drift. Although the network of Fig. 1B is well suited to the generation of a large diversity of axial activity patterns, it therefore appears to be a bad fit to biological observations. This led us to select the lamprey-inspired network of Fig. 1D for further investigations.

Gait transition in the flexible oscillator model

The model of the salamander spinal cord proposed by Ijspeert et al. (2007) was successful in reproducing important features of salamander locomotion, including the generation of traveling waves for swimming and standing waves for stepping. In the model, the formation of standing waves during stepping was caused by the extensive connections from limb to axial oscillators (Fig. 1A). The gap in frequencies between swimming and stepping observed in the animal was reproduced by using a lower intrinsic frequency for the limb oscillators, a hypothesis that was then verified in recordings of isolated parts of the spinal cord *in vitro* (Ijspeert et al. 2007). Finally, using a lower saturation threshold for the limb oscillators provided a mechanism for the automatic transition from stepping to swimming when the global excitatory drive was increased. This result mirrors the experimental observation that electrical stimulation of the mesencephalic locomotor region (MLR) can elicit swimming or stepping, depending on the strength of the electrical stimulus (Cabelguen et al. 2003).

The flexible CPG model of Fig. 1D can reproduce the transition between the swimming and stepping patterns without the extensive connections from limb to axial centers; only local connections are used. Instead, due to the mechanism of modulation of phase-lag described above, the lower intrinsic frequency of the limbs' centers can account both for the gap in frequencies between swimming and stepping *and* for the formation of a standing wave during stepping. To model the transition, we introduce a global excitatory drive signal d that represents the stimulation level in the MLR. This drive determines the intrinsic frequency and target amplitude of the oscillators:

$$v_i = \begin{cases} e_i d, & d < d_i^{th} \\ 0, & \text{otherwise} \end{cases}$$

$$R_i = \begin{cases} d, & d < d_i^{th} \\ 0, & \text{otherwise} \end{cases}$$

where d_i^{th} is the saturation threshold of oscillator i, and e_i a constant. Both d_i^{th} and e_i are set to lower values for limb oscillators than for axial oscillators. All parameter values are given in Table 1. With these

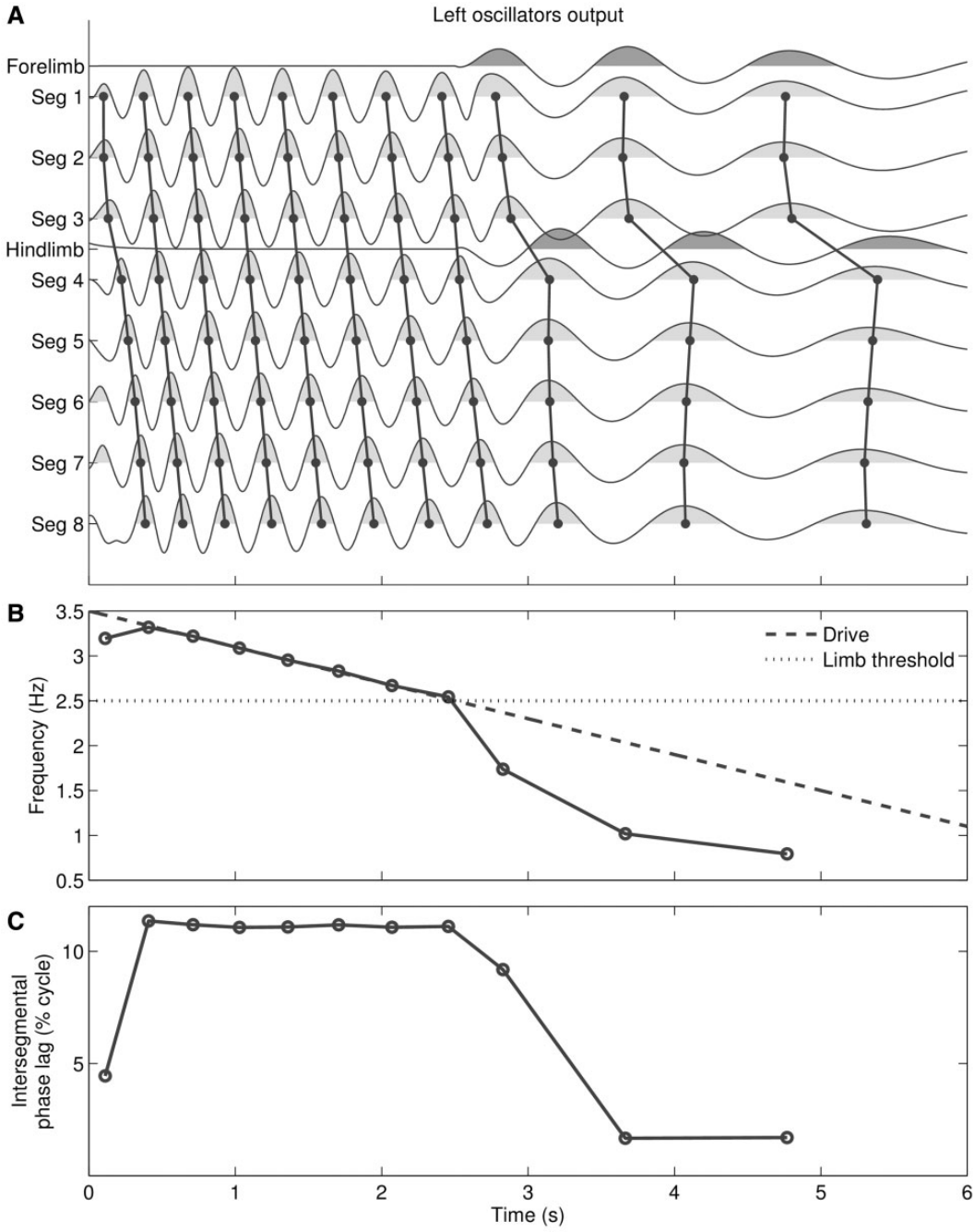

Fig. 6 Transition from swimming to walking in the oscillator model. The excitatory drive to the whole network is progressively decreased. (**A**) The output of oscillators for the left limbs (dark gray) and left hemicord (light gray) is shown, together with the lags between consecutive segments (thick lines). (**B**) The oscillation frequency (solid line) decreases linearly with the drive (dashed line), until the drive crosses the saturation threshold of the limb oscillators (dotted line) at which point the frequency drops abruptly. (**C**) As the limb oscillators come out of saturation, their influence on the trunk network causes a drop in intersegmental phase-lag from 11.1% to 1.7%.

values, the model reproduces the transition between swimming and stepping patterns with a simple decrease of the drive signal d as shown in Fig. 6.

A gait transition in the IF network

Aside from its utility as a robot controller (Ijspeert et al. 2007; Ijspeert 2008), the main aim of the modeling of the CPG is to gain a better understanding of the biological systems under study. Having found a flexible CPG network based on the abstract oscillator formalism, some important next steps are to validate the results with a less abstract model of the spinal network, to call attention to any difference in the results between these levels of abstraction, and

Table 2 Neuron parameters for the IF network

	Axial	Limb
E_{rest} (mV)	−70	−70
R (mΩ)	(89,91)	(85,86)
g	5.6	4.4
τ (ms)	150	150
α_1	45	25
α_2	15	15
$\Delta\omega_1$	0.99	0.65
$\Delta\omega_2$	0.025	0.025
$\tau_{\omega 1}$ (ms)	150	400
$\tau_{\omega 2}$ (ms)	2000	3200
$E_{revAMPA}$ (mV)	0	0
Δg_{AMPA}	0.1	0.1
τ_{AMPA} (ms)	20	20
$E_{revNMDA}$ (mV)	0	0
Δg_{NMDA}	0.1	0.1
τ_{NMDA} (ms)	100	100
$E_{revGLYC}$ (mV)	−85	−85
Δg_{GLYC}	0.1	0.1
τ_{GLYC} (ms)	20	20
Firing threshold (mV)	−38	−38

Parameters to the IF neurons used in this study. Pairs of numbers in parentheses indicate an interval from which values are sampled uniformly.

finally, to try to establish a correspondence between abstract oscillator models of CPGs and biologically detailed models (Kozlov et al. 2009; Bicanski et al. 2013b). To this end, we chose to compare the oscillator model of Fig. 1D to a CPG network composed of formal spiking neurons. The network depicted in Fig. 1E is composed of two types of segments, axial segments and simplified limb segments (see Bicanski et al. 2013b), that differ mainly in the time scales of adaptation (Table 2). Simulations of a biophysically detailed model of salamander spinal segments suggest that fast rhythms in the salamander, that is, *in vivo* activity, rely on adaptation for burst termination (Bicanski et al. 2013b). Blocking inhibitory connections between the hemisegments abolishes fast rhythms. In the lamprey, a similar mechanism may be involved in burst termination (Buchanan 1999; Jackson et al. 2005, however compare to Cangiano and Grillner 2003). In the present model, the time scale of adaptation determines the lower frequency range of oscillations for limb segments as compared with axial segments. Active limbs enforce these slower rhythms in the axis via local connections (see network 1, Table 3).

Figure 7 shows the gait transition for the IF network. The transition from swimming to stepping is achieved by a continuously decreasing drive to the axial network. Similarly to Ijspeert et al. (2007), the limb networks are silent during swimming. When the limbs come out of saturation, the intrinsically slower limb networks impose their frequency on the axis, leading to the characteristic jump in frequency (Fig. 7A(2)), and adjust the coordination pattern to produce a near-zero phase-lag (Fig. 7A(3)), that is, the standing wave typical for a stepping gait. The default network (network 1, see Fig. 7A(1–3) and Table 3) contains only descending intersegmental connections in the axis.

Adding ascending intersegmental connections (symmetric to the descending connections in terms of weights and connection probabilities) severely perturbs both gait patterns (network 2, see Fig. 7B(1) and Table 3). The added inhibitory connections to a given axial segment originating from caudally located segments slow down swimming oscillations and decrease the phase-lag. During the stepping stage, the inhibitory connections from the limb segments to the contralateral axial segments are not sufficient to suppress an upward traveling wave propagated by the newly added ascending connections. In the flexible oscillator model, perturbations to the pattern could be remedied by decreasing the weight of ascending connections by 80%. In the IF model, however, scaling the synaptic weights of ascending intersegmental connections has little to no effect, until the connections become so weak that their effect is negligible. On the other hand, reducing the number of rostrally directed intersegmental connections yields better results but does not allow for a clean stepping pattern in the trunk (network 2, see Fig. 7B(2) and Table 3).

To fully recover the gait transition, another adjustment to the connectivity is necessary to compensate for the out-of-phase excitation received by the last (i.e., most caudal) trunk segments due to ascending connections originating in the first tail segments. An additional inhibitory connection from the pelvic limb segment to the ipsilateral hemisegment located one segment rostrally (i.e., above the phase jump of π in the stepping pattern) restores the gait transition (network 3, see Fig. 7C(1–3) and Table 3). Alternatively to the addition of the new limb to axis connection, performance can also be restored by cutting the caudorostral intersegmental connections above the pelvic segment, that is, above the segment where the hind limbs project to the axis (network 4, not shown in Fig. 7, see Table 3).

Table 3 Connection densities and synaptic weights in the IF networks used in this study

	Network 1	Network 2	Network 3	Network 4
$E_{AX} \rightarrow E_{AX}$ ipsi +2	0 | 0	0.05 | 6,1.5	0 | 0	0 | 0
$E_{AX} \rightarrow E_{AX}$ ipsi +1	0 | 0	0.10 | 6,1.5	0.10 | 6,1.5	0.10 | 6,1.5
$E_{AX} \rightarrow E_{AX}$ ipsi 0	0.12 | 6,1.5	0.12 | 6,1.5	0.12 | 6,1.5	0.18 | 6,1.5
$E_{AX} \rightarrow E_{AX}$ ipsi −1	0.10 | 6,1.5	0.10 | 6,1.5	0.10 | 6,1.5	0.10 | 6,1.5
$E_{AX} \rightarrow E_{AX}$ ipsi −2	0.05 | 6,1.5	0.05 | 6,1.5	0.05 | 6,1.5	0.05 | 6,1.5
$E_{AX} \rightarrow I_{AX}$ ipsi 0	0.20 | 6,1.5	0.20 | 6,1.5	0.20 | 6,1.5	0.20 | 6,1.5
$I_{AX} \rightarrow ALL_{AX}$ contra +2	0 | 0	0.10 | 10	0.05 | 10	0.05 | 10
$I_{AX} \rightarrow ALL_{AX}$ contra +1	0 | 0	0.15 | 10	0.075 | 10	0.075 | 10
$I_{AX} \rightarrow ALL_{AX}$ contra 0	0.45 | 10	0.45 | 10	0.20 | 10	0.22 | 10
$I_{LI} \rightarrow ALL_{LI}$ contra 0	0.22 | 10	0.22 | 10	0.20 | 10	0.24 | 10
$I_{AX} \rightarrow ALL_{AX}$ contra −1	0.15 | 10	0.15 | 10	0.15 | 10	0.15 | 10
$I_{AX} \rightarrow ALL_{AX}$ contra −2	0.10 | 10	0.10 | 10	0.10 | 10	0.10 | 10
$E_{LI} \rightarrow ALL_{AX}$ ipsi 0	0.80 | 6,1.5	0.80 | 6,1.5	0.80 | 6,1.5	0.80 | 6,1.5
$E_{LI} \rightarrow ALL_{AX}$ ipsi −1	0.50 | 6,1.5	0.50 | 6,1.5	0.50 | 6,1.5	0.50 | 6,1.5
$I_{LI} \rightarrow ALL_{AX}$ contra 0	0.80 | 10	0.80 | 10	0.80 | 10	0.80 | 10
$I_{LI} \rightarrow ALL_{AX}$ contra −1	0.50 | 10	0.50 | 10	0.50 | 10	0.50 | 10
$I_{LI} \rightarrow ALL_{AX}$ ipsi +1	0 | 0	0 | 0	0.80 | 10	0 | 0

Pairs/triplets of numbers indicate connection density and synaptic weights (glycinergic or AMPA + NMDA), respectively. + indicates connections to segments above the reference segment, − indicates connections to segments below the reference segment. *E* and *I* denote excitatory and inhibitory neurons, respectively. ALL refers to all neurons in the ipsilateral (ipsi) or contralateral (contra) hemisegment. The subscripts AX and LI refer to axial and limb segments, respectively. Unless explicitly given, the intrasegmental connections for limb segments are the same as for axial segments. Network 1 (Fig. 7A): the default network as described in the text (only downward intersegmental coupling). Network 2 (Fig. 7A): the same as network 1 with added ascending intersegmental connections, symmetrical in weights, range, and connection density. Network 3 (Fig. 7A): the same as network 2, but with lower ascending connection density and an added connection from hind-limb inhibitory neurons to the ipsilateral hemisegment above the tail–trunk division. Network 4 (not shown in Fig. 7): the same as network 2, but with lower ascending connection density and no intersegmental ascending connections across the tail–trunk division.

Conclusion

Comparing models built at different levels of abstraction brings about many pitfalls. Yet, it is important to establish a chain of correspondent models, from abstract models all the way down to the lowest levels of abstraction (e.g., conductance-based models): linking different levels of modeling lends credibility to claims about biological systems that are made on the basis of abstract models.

We must be cautious, for instance, with the terms dominantly rostral and dominantly caudal for couplings, as they are defined in different ways in different models. In the work of Williams et al. (1990), who found evidence for dominantly ascending couplings in the lamprey CPG, coupling dominance was defined in abstract mathematical terms rather than relating directly to physiological properties. On the other hand, if one focuses on physiological aspects, several experimental and modeling studies support the notion of dominantly descending couplings in the lamprey spinal cord. Buchanan and co-workers have shown that intersegmental connections of both excitatory and inhibitory commissural interneurons project further in the caudal direction than in the rostral direction (Buchanan et al. 1989; Buchanan 2001). Several biologically detailed modeling studies on the lamprey spinal cord have used this type of coupling (Kozlov et al. 2007, 2009).

Caution is warranted when relating this anatomical interpretation of ''coupling dominance'' to the abstract mathematical framework of coupled oscillators. This is in part due to the fact that the match between oscillator coupling and synaptic connections is an imperfect one. Due to the type of phase-response curve used in the oscillator model, the effect of a particular coupling between two oscillators can be either to accelerate or to slow down the target (i.e., to advance or to delay the phase), depending on the target's state. Although the general mechanism of adjusting the phase lag transfers well between the models, a more systematic comparison between oscillator couplings and synaptic couplings among populations of neurons should be conducted.

For the lamprey, three intersegmental coupling schemes have been proposed that can potentially account for the intersegmental phase-lag: (i) a balanced ascending and descending coupling (Matsushima and

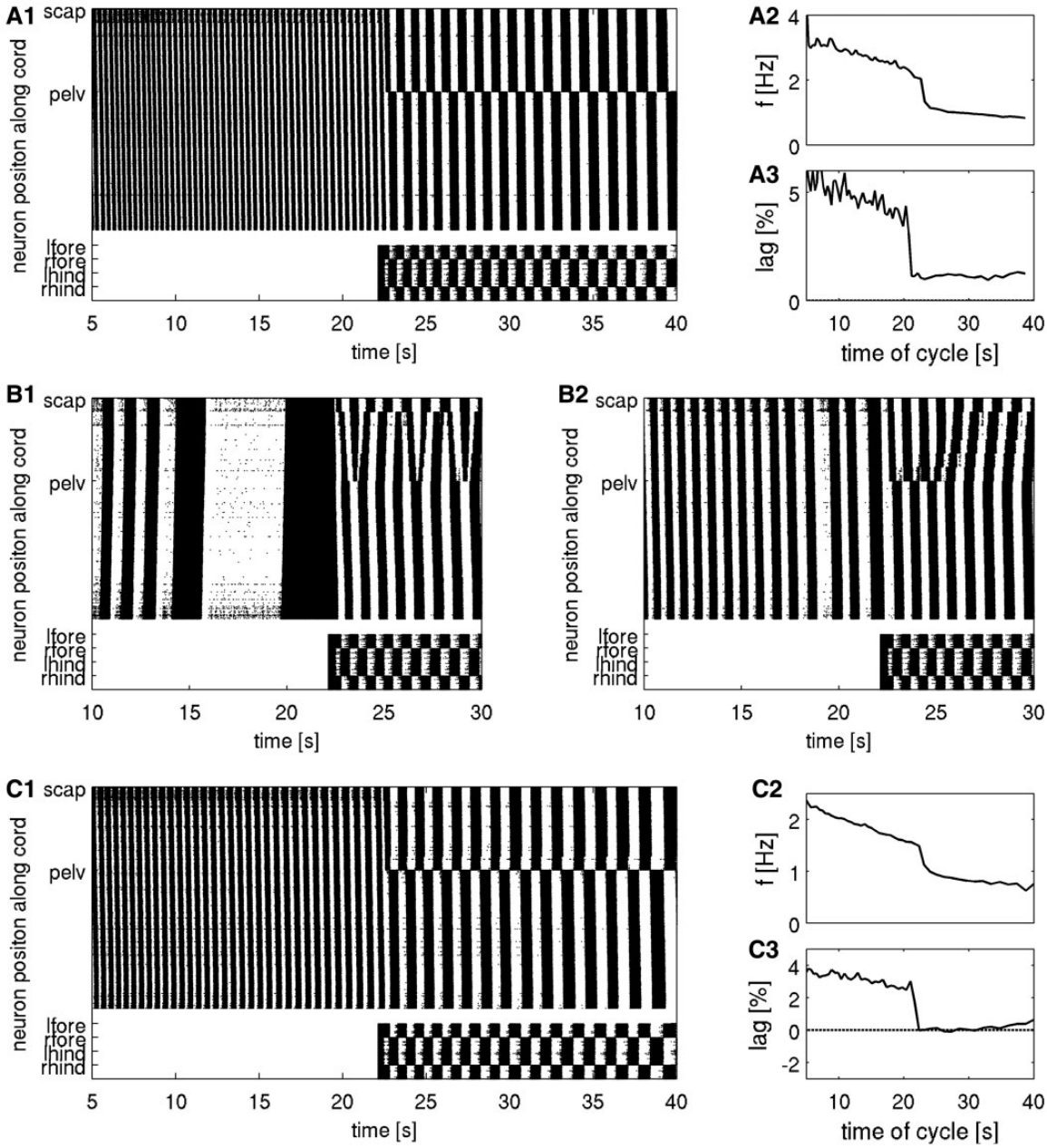

Fig. 7 Transition from swimming to stepping in IF networks. Panel groups **A** and **C** each show (1) a raster plot of the CPG network activity during the gait transition from swimming to stepping, (2) the frequency change from cycle to cycle during the transition, and (3) the change in phase-lag from cycle to cycle during the transition. (A) Network 1, only descending intersegmental connections (Table 3). (**B1**) Network 2, same as network 1 with the addition of balanced ascending connections (Table 3). (**B2**) Same as network 2 with decreased number of ascending connections. (**C**) Network 3, similarly to B2, the number of ascending projections has been decreased. In addition, inhibitory connections from the inhibitory hind-limb neurons to the ipsilateral hemisegment above the phase-jump have been added (Table 3). In all panel groups, the neurons are driven by injected current that is continuously decreased from 8.5 to 2.6 nA during the gait transition. Raster-plot labels indicate the scapular segment (*scap*) and the pelvic segment (*pelv*) along the spinal cord, as well as the left and right parts of the forelimb segment and hind-limb segment (*lfore, rfore, lhind, and rhind*).

Grillner 1992), based on observations that the spinal cord can be entrained by a leading rostral or caudal oscillator (“trailing oscillator” hypothesis); (ii) so-called dominantly descending coupling (Hagevik and McClellan 1994). This notion is supported by experiments in which pharmacological perturbation of the activity in the rostral spinal cord had strong effects on segments located caudally, whereas the opposite effect was weaker; (iii) so-called dominantly ascending coupling (Williams et al. 1990; Kopell et al. 1991; Cohen et al. 1992). This coupling scheme has been deduced from the observations

that the spinal cord can be entrained to a rhythm below the ''natural frequency'' of the cord by rhythmic bending of the caudal end, but not the rostral end (Williams et al. 1990).

In the models explored in the present work, balanced ascending and descending couplings in the axial network prohibit the simple adjustment of intersegmental phase-lag by changing the uncoupled frequency of the first segments. However, asymmetric couplings allow for a mechanism similar to that of the trailing oscillator hypothesis (Matsushima and Grillner 1992). When not in saturation, the limb networks assume the role of the leading oscillator, which slows down the network and decreases the phase-lag toward zero. This holds true at both levels of abstraction explored here.

The present work reproduces the transition of gait between swimming and stepping in the salamander. In contrast to the model of Ijspeert et al. (2007), it does so while preserving the flexibility of the axial network, allowing, for example, the formation of traveling waves of activity in the axis during stepping.

Our work suggests that the same principles that underlie the transitions between forward and backward swimming in models of the lamprey CPG could account for the transition between traveling waves of muscle activity during swimming and standing waves during stepping in the salamander.

Acknowledgments

Support for participation in this symposium was provided by the Society for Integrative and Comparative Biology; its Divisions of Animal Behavior, Comparative Biomechanics, Comparative Biology and Phylogenetics, Comparative Physiology and Biochemistry, Ecology and Evolution, Evolutionary Developmental Biology, Neurobiology, and Vertebrate Morphology; and the US National Science Foundation (IOS 1237547).

Funding

A.B. receives financial support from the Swiss initiative in systems biology: SystemsX.ch. D.R. received fellowships from the Fonds de la Recherche en Santé du Québec and the Groupe de Recherche sur le Système Nerveux Central. J.K., A.J.I., and J.-M.C. acknowledge support from the European Community (LAMPETRA Grant: FP7-ICT-2007-1-216100). J.-M.C. further receives support from the Fondation pour la Recherche Médicale (DBC 20101021008).

References

Bem T, Cabelguen J-M, Ekeberg Ö, Grillner S. 2003. From swimming to walking: a single basic network for two different behaviors. Biol Cybern 88:79–90.

Bicanski A, Ryczko D, Knuesel J, Harischandra N, Charrier V, Ekeberg Ö, Cabelguen J-M, Ijspeert AJ. 2013a. Decoding the mechanisms of gait generation in salamanders by combining neurobiology, modeling and robotics. Biol Cybern.

Bicanski A, Ryczko D, Knuesel J, Harischandra N, Charrier V, Ekeberg Ö, Cabelguen J-M, Ijspeert AJ. 2013b. From lamprey to salamander: an exploratory modeling study on the architecture of the spinal locomotor networks in the salamander. Biol Cybern.

Briggman KL, Kristan WB Jr. 2008. Multifunctional pattern-generating circuits. Annu Rev Neurosci 31:271–94.

Buchanan JT. 1999. Commissural interneurons in rhythm generation and intersegmental coupling in the lamprey spinal cord. J Neurophysiol 81:2037–45.

Buchanan JT. 2001. Contributions of identifiable neurons and neuron classes to lamprey vertebrate neurobiology. Prog Neurobiol 63:441–66.

Buchanan JT, McPherson DR. 1995. The neuronal network for locomotion in the lamprey spinal cord: evidence for the involvement of commissural interneurons. J Physiol 89:221–33.

Buchanan JT, Grillner S, Cullheim S, Risling M. 1989. Identification of excitatory interneurons contributing to generation of locomotion in lamprey: structure, pharmacology, and function. J Neurophysiol 62:59–69.

Buchanan J. 1982. Identification of interneurons with contralateral, caudal axons in the lamprey spinal cord: synaptic interactions and morphology. J Neurophysiol 47:961–75.

Cabelguen J-M, Ijspeert A, Lamarque S, Ryczko D. 2010. Axial dynamics during locomotion in vertebrates: lesson from the salamander. Prog Brain Res 187:149–62.

Cabelguen J-M, Bourcier-Lucas C, Dubuc R. 2003. Bimodal locomotion elicited by electrical stimulation of the midbrain in the salamander Notophthalmus viridescens. J Neurosci 23:2434–9.

Cangiano L, Grillner S. 2003. Fast and slow locomotor burst generation in the hemispinal cord of the lamprey. J Neurophysiol 89:2931–42.

Cheng J, Jovanovic K, Aoyagi Y, Bennett DJ, Han Y, Stein RB. 2002. Differential distribution of interneurons in the neural networks that control walking in the mudpuppy (Necturus maculatus) spinal cord. Exp Brain Res 145:190–8.

Cohen AH, Holmes PJ, Rand RH. 1982. The nature of the coupling between segmental oscillators of the lamprey spinal generator for locomotion: a mathematical model. J Math Biol 13:345–69.

Cohen AH, Ermentrout GB, Kiemel T, Kopell N, Sigvardt KA, Williams TL. 1992. Modelling of intersegmental coordination in the lamprey central pattern generator for locomotion. Trends Neurosci 15:434–8.

Delvolvé I, Bem T, Cabelguen JM. 1997. Epaxial and limb muscle activity during swimming and terrestrial stepping in the adult newt, Pleurodeles waltlii. J Neurophysiol 78:638–50.

Frolich L, Biewener A. 1992. Kinematic and Electromyographic Analysis of the Functional-Role of the Body Axis During Terrestrial and Aquatic Locomotion in the Salamander Ambystoma-Tigrinum. J Exp Biol 162:107–30.

Gao KQ, Shubin NH. 2001. Late Jurassic salamanders from northern China. Nature 410:574–7.

Grillner S. 2006. Biological Pattern Generation: the cellular and computational logic of networks in motion. Neuron 52:751–66.

Grillner S. 2003. The motor infrastructure: from ion channels to neuronal networks. Nat Rev Neurosci 4:573–86.

Hagevik A, McClellan AD. 1994. Coupling of spinal locomotor networks in larval lamprey revealed by receptor blockers for inhibitory amino acids: neurophysiology and computer modeling. J Neurophysiol 72:1810–29.

Harischandra N, Knuesel J, Kozlov A, Bicanski A, Cabelguen JM, Ijspeert AJ, Ekeberg Ö. 2011. Sensory feedback plays a significant role in generating walking gait and in gait transition in salamanders: a simulation study. Front Neurorobot 5:3.

Hill AA, Masino MA, Calabrese RL. 2003. Intersegmental coordination of rhythmic motor patterns. J Neurophysiol 90:531–8.

Ijspeert AJ. 2008. Special Issue: Central pattern generators for locomotion control in animals and robots: A review. Neural Networks 21:642–53.

Ijspeert AJ, Crespi A, Ryczko D, Cabelguen J-M. 2007. From swimming to walking with a salamander robot driven by a spinal cord model. Science 315:1416–20.

Ijspeert AJ, Crespi A, Cabelguen J-M. 2005. Simulation and robotics studies of salamander locomotion. Neuroinformatics 3:171–95.

Jackson AW, Horinek DF, Boyd MR, McClellan AD. 2005. Disruption of left–right reciprocal coupling in the spinal cord of larval lamprey abolishes brain-initiated locomotor activity. J Neurophysiol 94:2031–44.

Kopell N, Ermentrout GB, Williams TL. 1991. On Chains of Oscillators Forced at One End. SIAM J Appl Math 51:1397–417.

Kozlov A, Huss M, Lansner A, Kotaleski JH, Grillner S. 2009. Simple cellular and network control principles govern complex patterns of motor behavior. Proc Natl Acad Sci USA 106:20027–32.

Kozlov AK, Lansner A, Grillner S, Kotaleski JH. 2007. A hemicord locomotor network of excitatory interneurons: a simulation study. Biol Cybern 96:229–43.

Matsushima T, Grillner S. 1992. Neural mechanisms of intersegmental coordination in lamprey: local excitability changes modify the phase coupling along the spinal cord. J Neurophysiol 67:373–88.

McClellan AD, Sigvardt KA. 1988. Features of entrainment of spinal pattern generators for locomotor activity in the lamprey spinal cord. J Neurosci 8:133–45.

Nieuwenhuys R, Donkelaar HJ, Nicholson C, Smeets WJAJ. 1998. The central nervous system of vertebrates, 3 volume cased set with poster book. New York: Springer.

Rossignol S, Dubuc R, Gossard JP. 2006. Dynamic sensorimotor interactions in locomotion. Physiol Rev 86:89–154.

Ryczko D, Charrier V, Ijspeert A, Cabelguen JM. 2010a. Segmental Oscillators in Axial Motor Circuits of the Salamander: Distribution and Bursting Mechanisms. J Neurophysiol 104:2677–92.

Ryczko D, Dubuc R. 2013. The Multifunctional Mesencephalic Locomotor Region. Curr Pharm Des [Epub ahead of print].

Ryczko D, Dubuc R, Cabelguen J-M. 2010b. Rhythmogenesis in axial locomotor networks: an interspecies comparison. Prog Brain Res 187:189–211.

Ryczko D, Lamarque S, Didier H, Cabelguen JM. 2009. Dynamics of the axial locomotor network in the isolated spinal cord of the salamander. Soc Neurosci Program 565.8, Abstr. EE6.

Tråvén HG, Brodin L, Lansner A, Ekeberg Ö, Wallén P, Grillner S. 1993. Computer simulations of NMDA and non-NMDA receptor-mediated synaptic drive: sensory and supraspinal modulation of neurons and small networks. J Neurophysiol 70:695–709.

Vogels TP, Abbott LF. 2009. Gating multiple signals through detailed balance of excitation and inhibition in spiking networks. Nature Neurosci 12:483–91.

Williams TL, Sigvardt KA, Kopell N, Ermentrout GB, Remler MP. 1990. Forcing of coupled nonlinear oscillators: studies of intersegmental coordination in the lamprey locomotor central pattern generator. J Neurophysiol 64:862–71.